Bull. Mater. Sci., Vol. 10, No. 4, July 1988, pp. 313–322. © Printed in India.

Photoelectrochemical properties of metal-cluster oxide compounds, $A_2Mo_3O_8$ and $(LiY)Mo_3O_8$

M PARANTHAMAN, G ARAVAMUDAN and G V SUBBA RAO
Materials Science Research Centre, Indian Institute of Technology, Madras 600 036, India

Abstract. PEC studies on the single crystals of the metal-cluster oxide compounds, $A_2Mo_3O_8$ (A = Zn, Mg, Fe), and polycrystalline $LiYMo_3O_8$ are reported. The photoresponse behaviour is attributed to the Mo *d-d* transition. The photopotential, the photocurrent vs applied voltage and the wavelength data indicate that *n*-$Zn_2Mo_3O_8$ is stable and possesses a small and indirect band gap of 1·55 eV and a direct band gap of 1·9 eV. With change in A ions in $A_2Mo_3O_8$, there is no significant change in the PEC properties. $LiYMo_3O_8$ is found to be of *p*-type. PEC studies show that excepting for poor electronic conductivity, $A_2Mo_3O_8$ possesses all the requisite characteristics of an ideal photoanode for PAE of water for trapping solar energy.

Keywords. Metal-cluster oxides; *d-d* transition; single crystals; photoresponsive semiconductors.

1. Introduction

One of the chemical routes for trapping solar energy involves the photoassisted electrolysis (PAE) of water using a semiconducting oxide like *n*-TiO_2. Since the work of Fujishima and Honda (1972), a large number of binary and ternary oxide and non-oxidic materials have been studied for the conversion of solar energy into storable fuel, the hydrogen gas, in a single step. Efficiencies as high as 13% have been realized in PAE cells with *p*-InP, a non-oxidic material. The chemically stable oxidic materials possess large band gaps ($E_g \geqslant 3{\cdot}0$ eV) and do not absorb a significant portion of the solar spectrum. Hence, the maximum theoretical efficiency (η) obtainable is $\sim 7\%$ and experimentally realized is $\eta \sim 1\%$. Smaller band gap oxide materials ($E_g = 1{\cdot}5$–$2{\cdot}5$ eV) are not stable in aqueous alkali and acid electrolytes. For photoelectrochemical (PEC) reaction, apart from the intrinsic Fermi level, the quasi-Fermi level for holes is also important since the latter describes the oxidative power of the electrode under illumination. The quasi-Fermi level for photogenerated holes considers the entropy factor and is therefore dependent on the concentration of photogenerated holes Δp^*, as well as the band gap of the material (Alonso Vante and Tributsch 1986; Tributsch 1986). Usually, for oxides the valence band (VB) will be made up of oxygen (2*s*, 2*p*) orbitals. Hence, the effective mass (m_p^*) of the holes will be large and their mobility will be small ($\sim 0{\cdot}1 - 10^2$ cm^2/Volt. sec; e.g. $BaTiO_3$ has $\mu_p \sim 0{\cdot}3$ cm^2/Volt. sec). Several strategies have been adopted to improve the carrier mobilities. One strategy is to identify semiconducting materials with VB mainly of metal *d*-character. Here, the photogenerated holes produced from the narrow *d*-valence band can initiate better 'coordination' of OH^- or H_2O to the semiconductor surface. Hence, the electron transfer can take place easily. One can thus avoid the formation of free radicals like $OH^{\cdot}$ (which combine to give H_2O_2) as intermediates and the PAE reaction can proceed for the oxidation of water to molecular oxygen (Tributsch 1986). Since photoexcitation across the *d*-band (*d-d* transition) involves only mixing quasi-non-bonding electrons and if the *d*-bands are sufficiently broad (4*d*

or 5*d* bands rather than 3*d*-band materials), we can expect a higher hole mobility and thus larger Δp^* values. This strategy was first demonstrated for $LuRhO_3$ where Rh 4*d* filled-t_{2g} levels form the VB and 4*d*-e_g empty levels form the conduction band (CB). However, Jarrett *et al* (1980) employed $LuRhO_3$ as the cathode (*p*-$LuRhO_3$) for hydrogen evolution; detailed studies have not been made on the *n*-$LuRhO_3$ anode.

MoS_2 and the related transition metal dichalcogenides with the layer-structure are other examples of *d*-band materials extensively studied both with respect to physico-chemical (Subba Rao and Shafer 1979) and PEC properties (Alonso Vante and Tributsch 1986; Tributsch 1986). Compounds in which the metal atoms occur in pairs, triangular, tetra or octahedral clusters (cluster compounds) have unusual chemical and physical properties (Subba Rao and Geetha Balakrishnan 1984). Chemical bonding in the cluster compounds can range from covalent, metallic to ionic type. Tributsch and coworkers examined the PEC properties of Mo-cluster chalcogenide, $Mo_2Re_4Se_8$ and found good photocatalytic behaviour (Alonso Vante and Tributsch 1986; Tributsch 1986). We have recently examined the PEC behaviour of the metal cluster oxide compound, $Zn_2Mo_3O_8$ and found encouraging results (Paranthaman *et al* 1986a; Subba Rao *et al* 1986). In the present paper, we report on the detailed PEC studies of the isostructural series of compounds, $A_2Mo_3O_8$ (A = Mg, Fe, Zn) and $(LiY)Mo_3O_8$.

2. Structure and physical properties of $A_2Mo_3O_8$

$Zn_2^{2+}Mo_3^{4+}O_8$ is one example where there are a large number of isostructural hexagonal phases containing Mo_3-triangular clusters and where Mo is in apparently 4+ oxidation state and is present in an octahedral environment of oxide ions (figure 1) (Goodenough 1982; Ansell and Katz 1966). Zinc occupies both tetrahedral and octahedral interstices. $A_2Mo_3O_8$, A = Mg, Mn, Fe, Co, Ni and Cd, and $LiLnMo_3O_8$, Ln = Sm→Lu, Y, Sc are the other examples (DeBenedittis and Katz 1965; Ansell and Katz 1966; McCarroll 1977; McCarroll *et al* 1983).

In the latter series, Li and Ln occupy tetra- and octahedral voids respectively. In $A_2Mo_3O_8$, the intracluster Mo-Mo distances (~2·53 Å) are less than the Mo-Mo

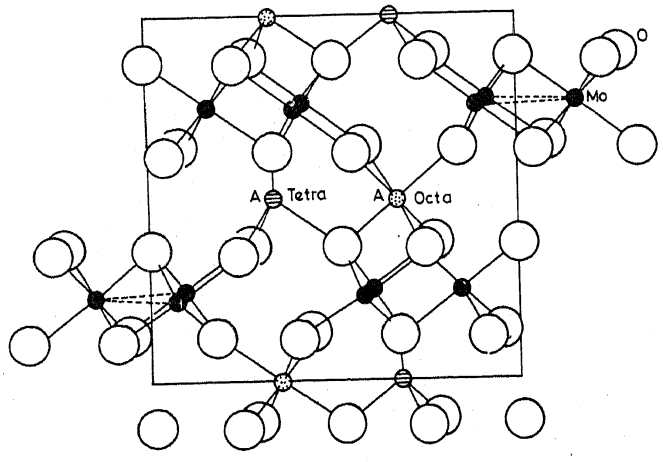

Figure 1. Crystal structure of $A_2Mo_3O_8$ showing the triangular Mo-clusters (after DeBenedittis and Katz 1965; Ansell and Katz 1966).

distance in molybdenum metal (~2·7 Å) and the inter-cluster distances are ~3·24 Å. Hence, there exists a strong metal-metal interaction leading to the formation of bands (rather than localized *d*-levels). The $A_2Mo_3O_8$ compounds with A = Mg, Zn, Cd and LiY are diamagnetic semiconductors or insulators indicating that the Mo-4*d* electrons are not localized and are present in a band (Goodenough 1982). Paramagnetic behaviour is noted in $A_2Mo_3O_8$ where A^{2+} = Mn, Fe, Co, Ni, the latter being paramagnetic ions (Goodenough 1982). The schematic band structure (one-electron energy band model diagram*) for $Zn_2Mo_3O_8$ shown in figure 2 can explain the observed diamagnetism and semiconductor behaviour. Optical band gaps of $A_2Mo_3O_8$ have not been reported in the literature; however, we can expect $E_g \sim$ 1·5–2·0 eV in comparison with other Mo-cluster compounds (e.g. $Mo_2Re_4S_8$, etc).

3. Experimental procedure

3.1 *Crystal growth by CVT*

Single crystals of $A_2Mo_3O_8$ (A = Zn, Mg and Fe) were grown by the fused salt electrolysis (FSE) and chemical vapour transport (CVT) techniques. For the CVT technique (Strobel *et al* 1982), starting molar ratios of corresponding metal oxides ZnO (99% pure; Loba), MgO (99·5% pure; Cerac, UK) or Fe_2O_3/Fe (JMC, UK; spec-pure) and MoO_2 (prepared by hydrogen reduction of MoO_3 at 480°C for 12 h) were mixed in the ratio of 1 : 1·6 along with $TeCl_4$ (transporting agent; 5 g/cc) and placed in an evacuated (10^{-5} torr) and sealed quartz tube (15 mm dia, 28 cm length). A three-zone furnace was used with temperature gradients 960–860–960°C and transport was carried out for 19 days. From the crystalline mass recovered after cooling and opening the quartz tube, shiny black crystals (cleaned by dil. HNO_3; up to a maximum of 3 × 3 mm platelets) were obtained. The hexagonal phase of $A_2Mo_3O_8$ was confirmed by powder X-ray diffraction (Philips Unit; Cu K_α radiation; 35 kV; 20 mA). The lattice parameters (e.g., $Zn_2Mo_3O_8$: a = 5·74; c = 9·88 Å) obtained were in good agreement with literature data (McCarroll 1977; Strobel *et al* 1982; McCarroll *et al* 1983).

3.2 *Crystal growth by FSE*

In the FSE method (McCarroll 1977; McCarroll *et al* 1983) crystals were obtained by the electrolysis of melts prepared from mixtures of sodium molybdate; molybdenum

*Construction of the band model diagram based on the Goodenough's (1982) approach is as follows: For oxygen, sp_σ hybrid orbitals and P_π orbitals are assumed. In an octahedral crystal field, the five-fold degenerate 4*d* orbitals are split into $3t_{2g}$ and $2e_g$ orbitals. The hybridized Mo-Metal $d^2sp^3(e_g)$ orbitals will combine with the oxygen sp_σ and P_π orbitals to form the valence and conduction bands. The non-bonding t_{2g} orbitals will form the π^* band due to significant overlap of 4*d*-Mo orbitals. Also, a trigonal component to the octahedral crystal field (due to oxide ions) splits the π^* band into singly degenerate a_{1g}^* and doubly degenerate e_g^* band. Zinc metal effects a charge transfer to the Mo-4*d* band and its 4*s*, 4*p* orbitals form an empty conduction band. Electron occupancy of each band (along with spin) is shown in brackets (figure 2). The total 70 electrons per formula unit (2Zn : 4; 3Mo : 18; 80 : 48) occupy a_{1g}^* band making it the VB and the $e_g^{\pi*}$ and other high lying bands the conduction band. The E_g, the distance on the energy scale between a_{1g}^* *and* $e_g^{\pi*}$ bands is low (~1·5–2·0 eV) making the compound $Zn_2Mo_3O_8$ a *d*-band semiconductor.

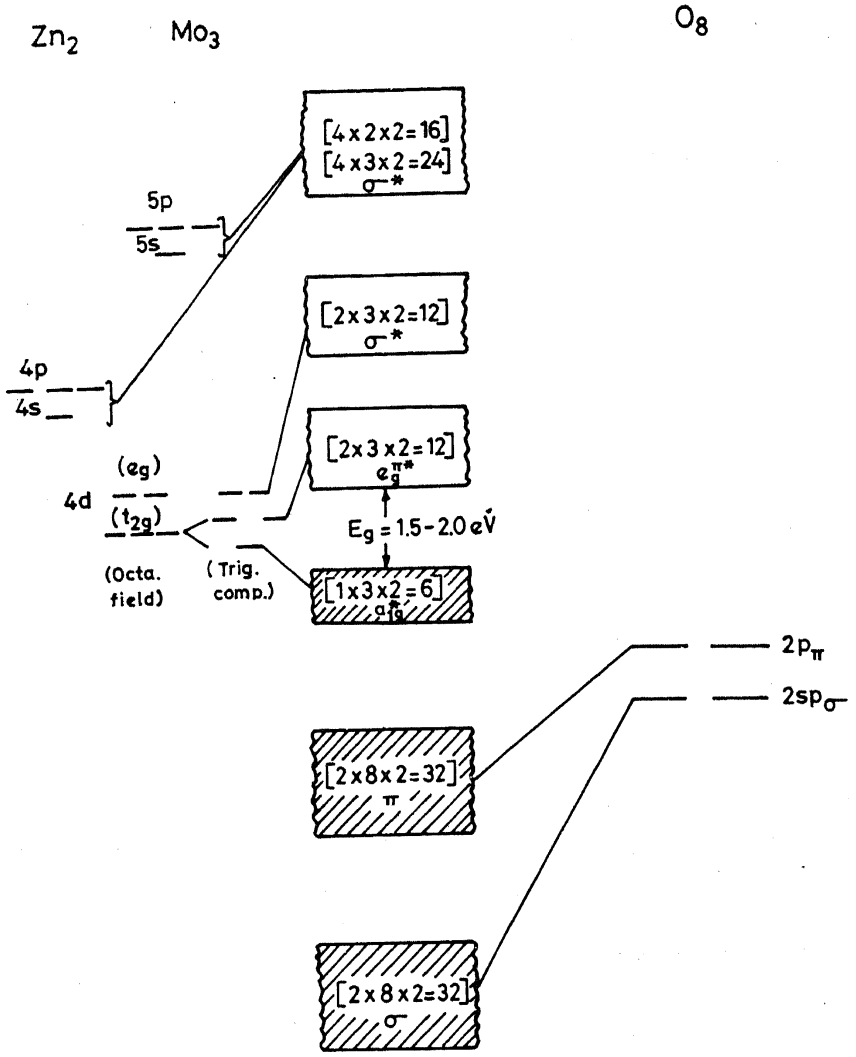

Figure 2. One-electron energy band diagram of $Zn_2Mo_3O_8$ showing the disposition of the VB and CB.

trioxide and the corresponding metal oxides (molar ratio = 1·0 : 1·0 : 1·5) at 1050°C. The reactants were weighed and mixed thoroughly in an agate mortar and transferred to a 20 ml Al_2O_3-crucible which was kept inside a vertical Kanthal-wound furnace. Two smooth platinum foil electrodes (~ 1 cm^2 area each) with 1·5 cm distance apart were inserted into the mixture. The alumina crucible was heated to 1050°C (over a period of 2 h) to allow the reactants to melt. The melt was then allowed to equilibrate for 1 h at 1050°C. A constant current of 200 mA and a cell potential of ~ 1V from a power supply (Aplab, India) was passed initially for 15 minutes for the nucleation of growth to occur. Subsequently, the current was reduced at the rate of 20 mA to 40 mA over 30 min intervals. After one hour, the electrolysis was stopped and the electrodes were removed from the melt and allowed to cool rapidly to room temperature in air. The products obtained at the cathode were then removed by dipping the electrodes in dil. HCl. Single crystals of hexagonal plates upto 4×2 mm size were obtained and confirmed by X-ray diffraction (McCarroll 1977; McCarroll *et al* 1983).

The detailed mechanism as to how the ternary oxide, $A_2Mo_3O_8$ is formed at the

cathode in the high temperature FSE is not known. The probable chemical reactions involved are:

Melt: $Na_2MoO_4 \rightarrow 2Na^+ + MoO_4^{2-}$ (ionization), (1)

At anode: $MoO_4^{2-} \rightarrow MoO_3 + 2e^- + \frac{1}{2}O_2$ (oxidation), (2)

At cathode: $2Na^+ + 2e^- \rightarrow 2Na$ (reduction; high potential), (3)

$2Na + 2MoO_3 \rightarrow Na_2MoO_4 + MoO_2$ (reduction; low or intermediate potential), (4)

and

$2Zn^{2+} + 3MoO_2 \rightarrow Zn_2Mo_3O_8$. (at cathode) (5)

The above reactions suggest that in the absence of Zn or when MoO_3 concentration is large, MoO_2 should be obtained, which is indeed observed experimentally during our runs as well as by others in the literature (McCarroll 1977; McCarroll *et al* 1983).

As-grown crystals had a high electrical resistance ($R \sim 10^5$ ohm). To enhance conductivity, preliminary experiments like H_2- reduction and Ti-gettering (in evacuated and sealed quartz tubes) were tried but those experiments resulted in the decomposition of the compound. Addition of scandium oxide (2·5 mol%; to replace Zn in $Zn_2Mo_3O_8$) during FSE resulted in some crystals possessing $R \sim 10^3$ ohm. However, with higher concentrations of added Sc_2O_3, blue coloured compounds (scandium molybdenum bronzes: Sc_xMoO_3) were obtained and the desired $Zn_2Mo_3O_8$ was not formed.

Efforts to grow single crystals for $LiYMo_3O_8$ by CVT and FSE methods were not successful. Polycrystalline $(LiY)Mo_3O_8$ was made by the solid state reaction of lithium molybdate (Li_2MoO_4), Y_2O_3 (99·99% pure; Indian Rare Earths), MoO_3 and Mo (JMC, spec-pure) in the stoichiometric proportions in an evacuated and sealed quartz tube at 700°C for 48 h. (DeBenedittis and Katz 1965). The compound was characterized by X-ray diffraction. Electrical studies showed it to be *p*-type with resistivity $\sim 10^4$ ohm. cm. at 300 K.

3.3 *PEC test set-up*

The $A_2Mo_3O_8$, A = Zn, Mg, Fe crystals and $LiYMo_3O_8$ were mounted and examined for their PEC behaviour. Aqua regia was used as the etchant solution. PEC studies were carried out in a 3-electrode configuration with a standard set-up described earlier (Paranthaman *et al* 1986b; Subba Rao *et al* 1984a). All the measured potentials are referenced to SCE.

4. Results and discussion

4.1 *PEC studies on $Zn_2Mo_3O_8$*

Detailed studies have been carried out for FSE and CVT crystals of $Zn_2Mo_3O_8$ of the PEC cell, $^{\oplus}n$-$Zn_2Mo_3O_8$/1 M NaOH (aq.) (pH = 13·3)/Pt$^{\ominus}$. Shifts in photopotential (negative sign indicating *n*-type behaviour of the anode) ranging from 400–500 mV for various crystals were noted. We also observed some dark potential

(~ -100 mV). Crystals obtained by FSE performed better. As shown in figure 3, the shifts in photopotential and short circuit photocurrent (i_{photo}) are very sharp and remain constant, without degradation, under full-light illumination with the 1000 W Xe-lamp. The sharp drop to the base-line with light 'off' is also an excellent indication that $Zn_2Mo_3O_8$ performs as a good photoanode. However, the i_{photo} values are small (0·14 mA/cm^2) because of their high resistance.

Potentiostatic I–V characteristics of n-$Zn_2Mo_3O_8$ in dark and illumination are shown in figure 4. Negligible dark currents are noted upto $-0{\cdot}1$ V and increase thereafter as the electrode is scanned towards anodic side. Significant photocurrents

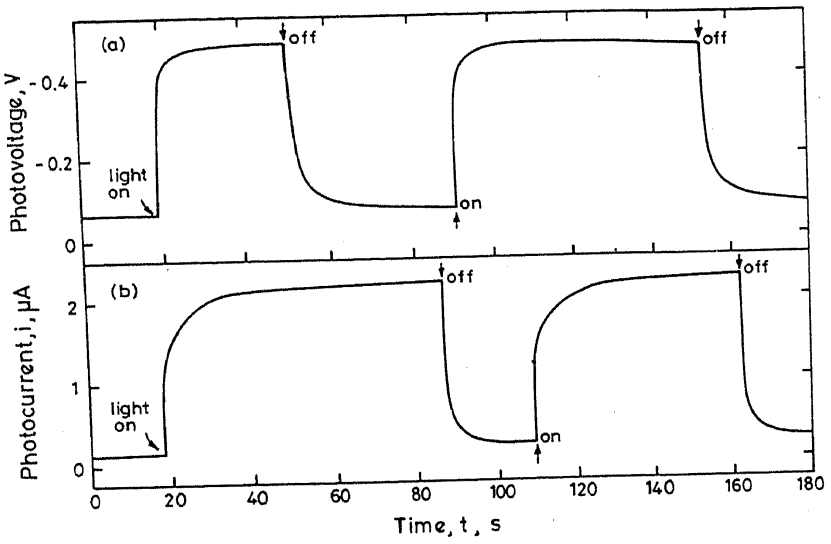

Figure 3. Photoresponse behaviour (recorder trace) or n-$Zn_2Mo_3O_8$ under dark and illumination in 1 M NaOH solution (1000 W Xe-lamp; full intensity $>1{\cdot}5$ W/cm^2; water filter): (**a**) shift in photopotential (vs. Pt), and (**b**) photocurrent at $-0{\cdot}2$ V vs SCE.

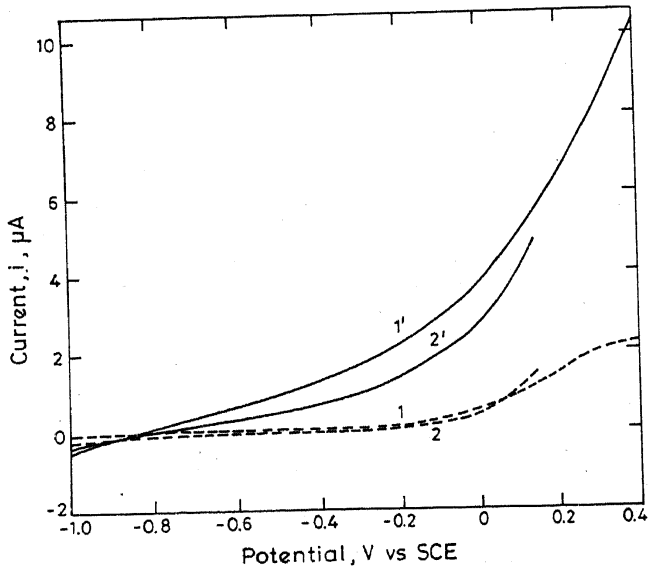

Figure 4. Potentiostatic current-voltage curves for the oxide electrodes in 1 M NaOH solution (pH = 13·3) with 1000 W Xe-lamp full intensity illumination; 1,1′: $Zn_2Mo_3O_8$; 2,2′: $Mg_2Mo_3O_8$. (1,2 dark 1′,2′ illuminated).

are obtained in the range −0·2 to +0·3 V, but no saturation occurs at the higher anodic potentials. Photocurrent onset occurs at −0·83 V at pH = 13·3, giving a rough value of V_{fb}. From the i^2_{photo} − V plot at a wavelength of 640 nm in 1 M NaOH solution, a correct value of V_{fb} of −0·79 V has been obtained (figure 5). V_{fb} shifts to more positive values with decrease in pH of the electrolyte solution by 0·06 V/pH unit. We have not been successful in obtaining reliable and reproducible capacitance data on $Zn_2Mo_3O_8$.

From the normalized photocurrent vs wavelength curves determined at −0·2 V in 1 M NaOH, quantum efficiency [Φ_e, defined as (i_{photo}/eF_0), where e is the electronic charge and F_0, the photon flux] obtained are low (0·3% at 500 nm) (figure 6). This is definitely due to the high resistance of the as-grown $Zn_2Mo_3O_8$ crystals. The onset of photocurrent occurs at $\lambda = 770 - 780$ nm, corresponding to an E_g of ~1·6 V. The spectral response data of figure 6 are replotted as $(\Phi_e h\nu)^{0.5}$ vs $h\nu$ (eV) (Butler and Ginley 1980) to get a straight line plot to extrapolate to a value of 1·55 eV showing that $Zn_2Mo_3O_8$ is an indirect band gap semiconductor (figure 7a). The $(\Phi_e h\nu)^2$ vs $h\nu$ plot gives another (viz. direct) band gap at 1·9 eV for $Zn_2Mo_3O_8$ (figure 7b).

We must point out that the existence of an indirect as well as direct band gap in a semiconductor should show up as an abrupt change in slope of the quantum efficiency vs wavelength curve. Besides, straight plots of $(\Phi h\nu)^{0.5}$ *and* $(\Phi h\nu)^2$ vs $h\nu$ should be obtained in two different, but non-overlapping, spectral regions. Examples where both direct and indirect band gaps are encountered in the same material are: CdO (Benko and Koffyberg 1986); $Sr_2Nb_2O_7$ and $Ba_{0.5}Sr_{0.5}Nb_2O_6$ (Hormadaly *et al* 1980). However, in the present case of $Zn_2Mo_3O_8$ and $Mg_2Mo_3O_8$, abrupt changes in slope have not been encountered as can be seen from figure 6. Possibly, the observed behaviour seen in figure 6 may indicate defect-related sub-band gap states extending from the band edges into the band gap as illustrated by the work of Butler *et al* (1981) and Salvador *et al* (1984) although the nature and origin of these states may differ for the present compounds. Since many *d*-band semiconductors exhibit predominantly indirect band gaps (e.g. MoS_2, $Mo_2Re_4Se_8$), we may also expect $Zn_2Mo_3O_8$ to exhibit an indirect gap rather than direct band gap.

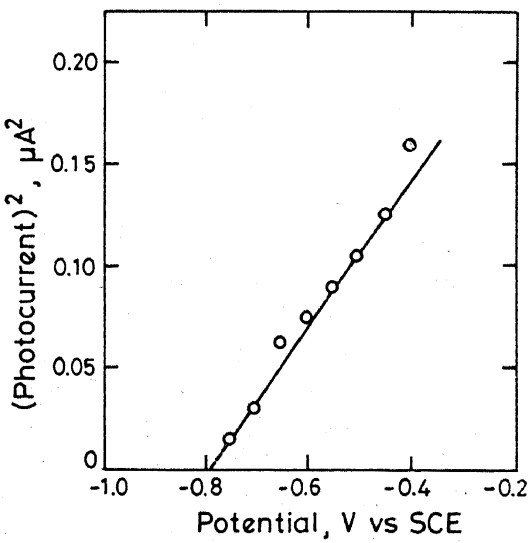

Figure 5. i^2_{photo} vs V plot for $Zn_2Mo_3O_8$ in 1 M NaOH solution. Data taken at a wavelength of 640 nm using filter. The data points are LSQ fitted to extrapolate to V_{fb}.

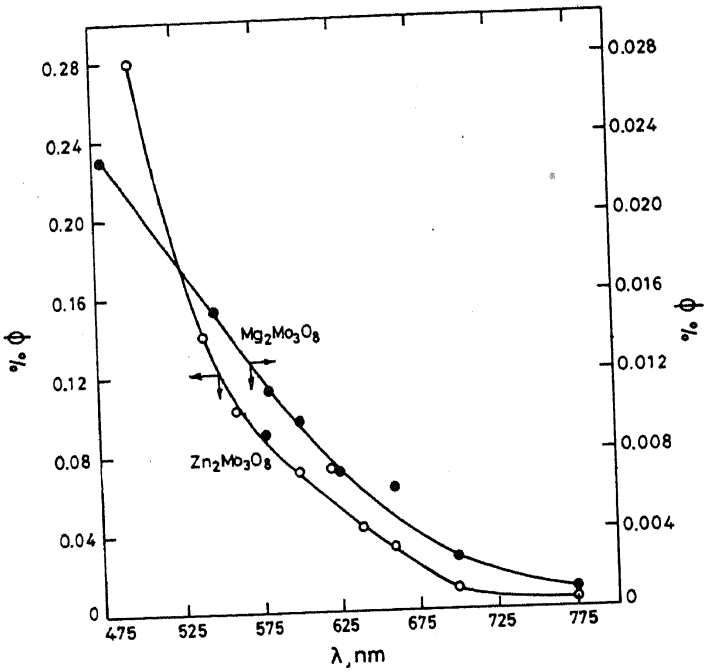

Figure 6. Quantum efficiency vs wavelength for the oxide electrodes in 1 M NaOH at −0·2 V vs SCE. The data points are taken using filters.

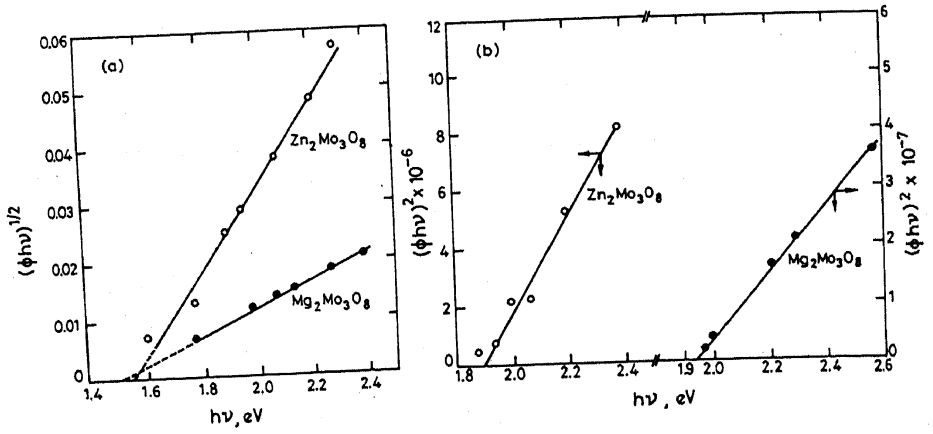

Figure 7. Determination of (**a**) indirect band gap from $(\Phi_e h\nu)^{0.5}$ vs $h\nu$ plot and (**b**) direct band gap from $(\Phi_e h\nu)^2$ vs $h\nu$ plot for the oxide electrodes. The data points are LSQ fitted for extrapolation.

Long-term stability experiments have shown that $Zn_2Mo_3O_8$ is stable for atleast 6 h in 1 M NaOH and in neutral solutions under illumination (figure 8). Due to the smaller photocurrents (0·2 mA/cm^2), we have not been able to observe oxygen evolution at the electrode. With scandium-doped $Zn_2Mo_3O_8$ FSE crystals, there is no improvement in the PEC performance because their resistance is still in the higher order as mentioned above. In addition to 1 M NaOH electrolyte solution, preliminary experiments were carried out in I_2/I_n^- and $Fe(CN)_6^{4-/3-}$ electrolytes with the *n*-$Zn_2Mo_3O_8$ photoanode. The photoresponse was sluggish and we could not get reliable data. This is probably due to the poor electrical conductivity of these samples.

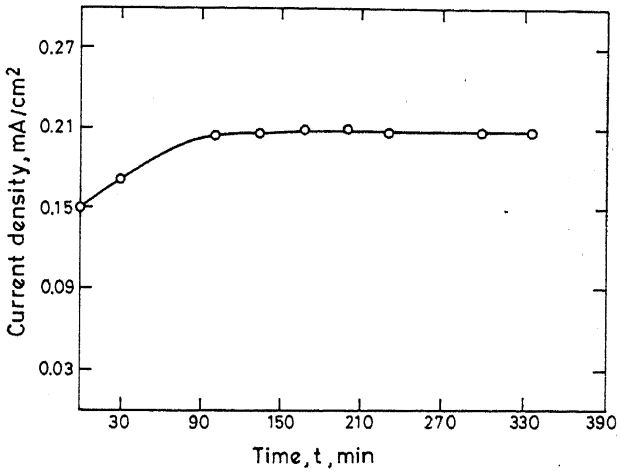

Figure 8. Photocurrent density vs time plot for $ZnMo_3O_8$ in 1 M NaOH at −0·2 V vs SCE under 1000 W Xe-lamp illumination.

4.2 *PEC studies on $Mg_2Mo_3O_8$, $Fe_2Mo_3O_8$ and $(LiY)Mo_3O_8$*

$Mg_2Mo_3O_8$ and $Fe_2Mo_3O_8$ also exhibit excellent photo-response behaviour similar to $Zn_2Mo_3O_8$. The maximum V_{OC} values of 250 and 180 mV (vs Pt) have been observed in 1 M NaOH. The shifts are towards greater negative potentials typical of *n*-type semiconductors. We also have observed significant dark potentials (−100 mV) similar to $Zn_2Mo_3O_8$. Potentiostatic I-V curve for $Mg_2Mo_3O_8$ is shown in figure 4. As in $Zn_2Mo_3O_8$, dark currents are smaller upto −0·2 V and increase thereafter in the anodic region. The increased dark current could be due to the Mo^{4+} present in $A_2Mo_3O_8$ getting oxidized to Mo^{6+}. Cyclic voltammograms in the dark in highly alkaline medium in fact showed anodic oxidation peak above +0·2 V in many $A_2Mo_3O_8$ crystals and a reversible reduction peak near +0·0 V. However, detailed studies have not been made. Significant photocurrents are obtained in the range −0·3 to +0·1 V but no saturation occurred in $Mg_2Mo_3O_8$. Photocurrent onset occurs at −0·83 V ($\approx V_{fb}$). Similar I-V behaviour is observed with $Fe_2Mo_3O_8$ but the photocurrent onset occurred at −0·6 V.

From the normalized photocurrent vs wavelength relation, determined at −0·2 V in 1 M NaOH, a very low quantum efficiency of 0·015% at 500 nm has been found for $Mg_2Mo_3O_8$ (figure 6). The $(\Phi_e h\nu)^{0.5}$ vs $h\nu$(eV) curve shows that $Mg_2Mo_3O_8$ is an indirect band gap semiconductor with $E_g = 1{\cdot}50$ eV (figure 7a). However, the comments earlier made regarding $Zn_2Mo_3O_8$ apply equally well to $Mg_2Mo_3O_8$.

Thus, PEC studies of the isostructural series of the metal-cluster oxide compounds of the $A_2Mo_3O_8$ show that there is no significant change in the band gap position and PEC properties with change in A ions (A = Zn, Mg, Fe, etc.). Preliminary studies on $(LiY)Mo_3O_8$ show *p*-type behaviour (shift in photopotential towards greater positive direction) with a V_{OC} of ~90 mV in 1 M NaOH solution. Since it behaves like a photocathode, further experiments have not been pursued.

5. Conclusions

Metal-cluster oxide compounds of the series $A_2Mo_3O_8$ (A = Zn, Mg, Fe, etc) perform

as good photoanodes for the PAE of water for trapping solar energy. The photoresponse behaviour in $A_2Mo_3O_8$ series is attributed to the molybdenum *d-d* transition with a small and indirect band gap of 1·5–1·6 eV. $LiYMo_3O_8$ was found to be of *p*-type. Long-term stability (under illumination) studies indicate that $Zn_2Mo_3O_8$ is stable for atleast 6 h in alkali and in neutral solutions. With change in A ions (A = Zn, Mg, Fe, etc) in $A_2Mo_3O_8$, there is no change in the PEC properties. Improvements are perhaps possible if the electronic resistivities of these compounds are optimized by Li-insertion or by doping part of Zn by M^{3+} ions. Doping with Sc^{3+}, however, gave poor results.

Acknowledgements

Thanks are due to the referee for valuable comments and helpful suggestions. Thanks are due to the Department of Non-Conventional Energy Sources, Government of India, New Delhi, for the award of a research grant. MP acknowledges the award of a CSIR fellowship.

References

Alonso Vante N and Tributsch H 1986 *Proc. Sixth Int. Conf. on Photochemical Conversion and Storage of Solar Energy, Paris, Paper C-79*

Ansell G B and Katz L 1966 *Acta Crystallogr.* **21** 482

Benko F A and Koffyberg F P 1986 *Solid State Commun.* **57** 901

Butler M A, Abramovich M, Decker F and Juliao J F 1981 *J. Electrochem. Soc.* **128** 200

Butler M A and Ginley D S 1980 *J. Mater. Sci.* **15** 1

DeBenedittis J and Katz L 1965 *Inorg. Chem.* **4** 1836

Goodenough J B 1982 *Proc. Climax Fourth Int. Conf. on Chem. and uses of Mo* (eds) H F Barry and P C M Mitchell (Ann. Arbor, Michigan: Climax Molybdenum Co.)

Hormadaly J, Subbarao S N, Kershaw R, Dwight K and Wold A 1980 *J. Solid State Chem.* **33** 27

Jarrett H S, Sleight A W, Kung H H and Gillson J L 1980 *J. Appl. Phys.* **51** 3916

McCarroll W H 1977 *Inorg. Chem.* **16** 3353

McCarroll W H, Darling C and Jakubicki G 1983 *J. Solid State Chem.* **48** 189 and references therein

Paranthaman M, Aravamudan G and Subba Rao G V 1986a *Indian J. Technol.* **24** 399

Paranthaman M, Aruchamy A, Aravamudan G and Subba Rao G V 1986b *Mater. Chem. Phys.* **14** 349

Salvador P, Gutierrez C, Campet G and Hagenmuller P 1984 *J. Electrochem. Soc.* **131** 550

Strobel P, Le Page Y and McAlister S P 1982 *J. Solid State Chem.* **42** 242

Subba Rao G V, Aruchamy A, Aravamudan G and Paranthaman M 1984 *Advances in hydrogen energy 4. Hydrogen energy progress* (New York: Pergamon Press) vol. 3, p. 1075

Subba Rao G V and Geetha Balakrishnan 1984 *Bull. Mater. Sci.* **6** 283

Subba Rao G V, Paranthaman M and Aravamudan G 1986 *Proc. Sixth Int. Conf. on Photochemical Conversion and Storage of Solar Energy, Paris,* Paper D-103

Subba Rao G V and Shafer M W 1979 in *Physics and chemistry of materials with layered structures* (ed.) F Levy (Dordrecht: D. Reidel) vol. 6

Tributsch H 1986 in *Modern aspects of electrochemistry* No. 17 (eds) J O'M Bockris, B E Conway and R E White (New York: Plenum) p. 303